npj | Quantum Materials

www.nature.com/npjquantmats

ARTICLE OPEN

Check for updates

Non-local effect of impurity states on the exchange coupling mechanism in magnetic topological insulators

Thiago R. F. Peixoto[1]✉, Hendrik Bentmann[1], Philipp Rüßmann[2], Abdul-Vakhab Tcakaev[3], Martin Winnerlein[4], Steffen Schreyeck[4], Sonja Schatz[1], Raphael Crespo Vidal[1], Fabian Stier[3], Volodymyr Zabolotnyy[3], Robert J. Green[5,6], Chul Hee Min[1,7], Celso I. Fornari[1], Henriette Maaß[1], Hari Babu Vasili[8], Pierluigi Gargiani[8], Manuel Valvidares[8], Alessandro Barla[9], Jens Buck[10], Moritz Hoesch[10], Florian Diekmann[7], Sebastian Rohlf[7], Matthias Kalläne[7,11], Kai Rossnagel[7,10,11], Charles Gould[4], Karl Brunner[4], Stefan Blügel[2], Vladimir Hinkov[3], Laurens W. Molenkamp[4] and Friedrich Reinert[1]

Since the discovery of the quantum anomalous Hall (QAH) effect in the magnetically doped topological insulators (MTI) Cr:(Bi,Sb)$_2$Te$_3$ and V:(Bi,Sb)$_2$Te$_3$, the search for the magnetic coupling mechanisms underlying the onset of ferromagnetism has been a central issue, and a variety of different scenarios have been put forward. By combining resonant photoemission, X-ray magnetic circular dichroism and density functional theory, we determine the local electronic and magnetic configurations of V and Cr impurities in (Bi,Sb)$_2$Te$_3$. State-of-the-art first-principles calculations find pronounced differences in their 3*d* densities of states, and show how these impurity states mediate characteristic short-range *pd* exchange interactions, whose strength sensitively varies with the position of the 3*d* states relative to the Fermi level. Measurements on films with varying host stoichiometry support this trend. Our results explain, in an unified picture, the origins of the observed magnetic properties, and establish the essential role of impurity-state-mediated exchange interactions in the magnetism of MTI.

npj Quantum Materials (2020)5:87 ; https://doi.org/10.1038/s41535-020-00288-0

INTRODUCTION

Magnetically doped topological insulators (MTI) form a cornerstone in the field of topological quantum materials. Particularly in Cr-doped and V-doped (Bi,Sb)$_2$Te$_3$, the combination of ferromagnetism and a topologically non-trivial electronic band structure led to the discovery of the quantum anomalous Hall (QAH) effect[1–5], i.e. a dissipationless quantised edge-state transport in the absence of external magnetic fields. These materials are now being widely utilised for possible realisations of topological superconductor[6] and axion insulator states[7], as well as in the context of metrology[8] and spintronic functionalities[9]. However, despite the broad interest in these dilute MTI, controversy still remains as to the microscopic origin of the ferromagnetism and to the electronic states inducing the ferromagnetic (FM) coupling.

In a pioneering work, predicting the QAH effect in transition metal (TM)-based MTI, the FM state was proposed to arise from a van Vleck mechanism, as a result of strong spin–orbit coupling (SOC) and the topologically non-trivial band ordering in these materials[10]. Although some experimental support for this scenario has been reported[2,11,12], more recent first-principles calculations find that the strength of the exchange interactions in Cr:(Bi,Sb)$_2$Te$_3$ and V:(Bi,Sb)$_2$Te$_3$ is, in fact, largely independent of SOC, suggesting that the van Vleck mechanism, in the form proposed in ref. [10], plays no decisive role[13,14]. Other theoretical works predict a dependence of the magnetic coupling on the precise configuration of the impurity 3*d* states[13–18], as it is known in the context of dilute magnetic semiconductors[19–24]. Experimentally, the robustness of the FM state in Cr:(Bi,Sb)$_2$Te$_3$ and V:(Bi,Sb)$_2$Te$_3$ films was indeed found to vary substantially with dopant type and host stoichiometry[3,25–31]. It was speculated that these variations arise from differences in the electronic structure of the two systems[3]. So far, however, a comprehensive understanding of how this behaviour is related to the local impurity electronic structure is still absent. A realistic theory of the impurity 3*d* states in MTI shall not only explain the differences observed in the electronic and magnetic properties of these two coined QAH insulators, but also bring important insights for the physical description of other MTI, with possible implications to other TM-based van der Waals materials.

In this work, we present a combination of key experiments and theory that establishes the fundamental link between local impurity electronic structure and magnetic coupling in MTI. By means of X-ray magnetic circular dichroism (XMCD) and resonant photoelectron spectroscopy (resPES) we systematically probe the electronic and magnetic fingerprints of the 3*d* states of V and Cr impurities embedded in the bulk of (Bi$_x$Sb$_{1-x}$)$_2$Te$_3$ thin films, as well as the effect of Bi/Sb substitution in the host. Supported by multiplet ligand field theory (MLFT) and ab initio density functional theory (DFT) calculations, our results unveil the essential role of impurity-state-mediated exchange interactions underlying the magnetic properties of V-doped and Cr-doped (Bi,Sb)$_2$Te$_3$ thin

[1]Experimentelle Physik VII and Würzburg-Dresden Cluster of Excellence ct.qmat, Fakultät für Physik und Astronomie, Universität Würzburg, Am Hubland, D-97074 Würzburg, Germany. [2]Peter Grünberg Institut (PGI-1) and Institute for Advanced Simulation (IAS-1), Forschungszentrum Jülich and JARA, D-52425 Jülich, Germany. [3]Experimentelle Physik IV and Röntgen Research Center for Complex Materials (RCCM), Fakultät für Physik und Astronomie, Universität Würzburg, Am Hubland, D-97074 Würzburg, Germany. [4]Experimentelle Physik III and Institut für Topologische Isolatoren, Fakultät für Physik und Astronomie, Universität Würzburg, Am Hubland, D-97074 Würzburg, Germany. [5]Department of Physics and Astronomy and Stewart Blusson Quantum Matter Institute, University of British Columbia, Vancouver BC V6T 1Z4, Canada. [6]Department of Physics and Engineering Physics and Centre for Quantum Topology and Its Applications (quanTA), University of Saskatchewan, Saskatoon SK S7N 5E2, Canada. [7]Institut für Experimentelle und Angewandte Physik, Christian-Albrechts-Universität zu Kiel, D-24098 Kiel, Germany. [8]ALBA Synchrotron Light Source, E-08290 Cerdanyola del Vallès, Spain. [9]Istituto di Struttura della Materia (ISM), Consiglio Nazionale delle Ricerche (CNR), Trieste I-34149, Italy. [10]Deutsches Elektronen-Synchrotron DESY, D-22607 Hamburg, Germany. [11]Ruprecht Haensel Laboratory, Kiel University and DESY, D-24098 Kiel and D-22607, Hamburg, Germany. ✉email: Thiago.Peixoto@physik.uni-wuerzburg.de

films, paving the way towards a more general theory of the magnetic interactions in MTI.

RESULTS

Electronic and magnetic ground state of V and Cr impurities

We start by presenting in Fig. 1a, b the X-ray absorption (XAS) and XMCD spectra from $V_{0.1}(Bi_{0.32}Sb_{0.68})_{1.9}Te_3$ and $Cr_{0.1}(Bi_{0.1}Sb_{0.9})_{1.9}Te_3$, respectively, at the V and Cr $L_{2,3}$ edges, measured at temperatures above (hollow circles) and below (full circles) the Curie temperature T_C (Supplementary Fig. 1). No energy shifts or changes in the branching ratio are observed at the $L_{2,3}$ edges with varying temperature across T_C, contradicting recent reports where an apparent energy shift was interpreted as evidence of the van Vleck mechanism[11]. The XMCD spectra were measured under a small applied magnetic field of 10 mT (remanent state), oriented perpendicular to the surface, at 5 K. They confirm a persistent FM state at this temperature, with a sizable magnetic moment carried by the TM 3*d* states for both V-doped and Cr-doped (Bi, Sb)$_2$Te$_3$ systems.

A state-of-the-art MLFT analysis of the V and Cr $L_{2,3}$ lineshapes has been performed (Supplementary Fig. 1) and described in detail elsewhere[32]. We find a strong deviation from the 3+ ionic (V d^2, Cr d^3) ground state[25,29,30], with resulting *d*-shell occupations of $d^{3.13}$ ($m_S = 2.33\mu_B$ per atom) for V and $d^{4.37}$ ($m_S = 3.32\mu_B$ per atom) for Cr. Correspondingly, our first-principles calculations for single V and Cr impurities embedded in a quintuple layer of Sb_2Te_3, on an octahedral Sb site, find $d^{3.35}$ ($m_S = 2.51\mu_B$ per atom) and $d^{4.40}$ ($m_S = 3.72\mu_B$ per atom), (Supplementary Fig. 5 and below). This implies a substantial charge transfer (CT) from the ligand *p* states into the 3*d* impurity states as a result of strong *pd* hybridisation (Supplementary Fig. 4).

Fingerprint of the impurity 3*d* states

We next assess the contribution of the 3*d* states to the valence band (VB) by resPES at the V and Cr L_3 edges. The data sets shown in Fig. 2a, b are obtained from the normalised difference between the on-resonant and off-resonant photoemission spectra, taken at 30 K (Supplementary Fig. 2), and represent the V and Cr 3*d* partial DOS. The data establish a remarkably pronounced difference in the character of the 3*d* DOS for V and Cr impurities. For V, the 3*d* states pile up predominantly in a narrow peak just below E_F with the centre at $E_B = 170$ meV. For Cr, on the other hand, the 3*d* states are broadly distributed over the host VB, with a maximum at $E_B = 1.71$ eV and low spectral weight near E_F. Our first-principles calculations nicely capture these main characteristics. Figure 2c shows the calculated spin-polarised 3*d* DOS and the corresponding integrated DOS for V (upper panel) and Cr (lower panel) impurities in Sb_2Te_3, which allow us to assign the experimentally observed states to majority-spin (spin-up) t_{2g} states (Supplementary Fig. 6). The examination of the integrated 3*d* DOS at E_F allows us to extract the predicted *d*-shell filling of $d^{3.4}$ for V (red curve) and $d^{4.4}$ for Cr (blue curve) impurities, in good agreement with our MLFT analysis. Furthermore, our calculations are able to reproduce our resPES data without self-interaction corrections, which suggests a minor role of the latter for the V and Cr occupied 3*d* states. While small self-interaction corrections tend to shift the 3*d* resonances deeper in the VB[13,14,18,21], this is compensated by the natural charge doping of the host, as we discuss below. Our findings yet support previous resPES results[33,34], and recent scanning tunnelling microscopy and spectroscopy studies of the electronic fingerprints of substitutional V and Cr impurities in Sb_2Te_3[18,35,36].

The presence of exchange-split 3*d* states at E_F suscitate the emergence of localised magnetic moments and, possibly, long-range magnetic order. In order to study the effect of the impurity states on the magnetic coupling mechanism, we first consider the

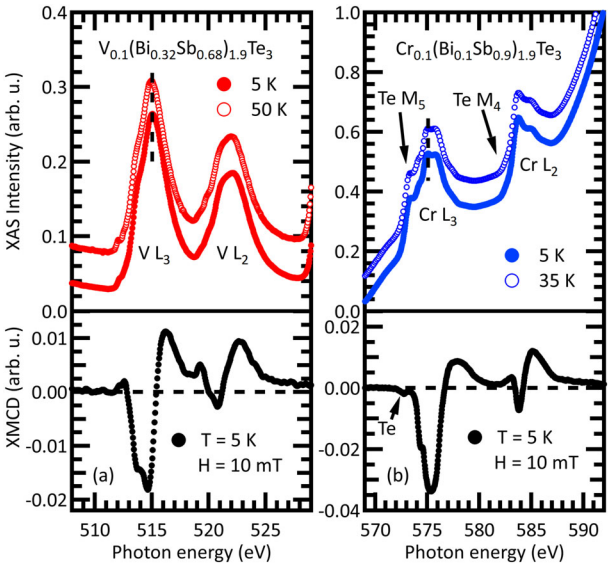

Fig. 1 Magnetic fingerprints of V and Cr impurities in (Bi,Sb)$_2$Te$_3$. XAS (upper panels) and XMCD (lower panels) spectra of **a** $V_{0.1}(Bi_{0.32}Sb_{0.68})_{1.9}Te_3$ and **b** $Cr_{0.1}(Bi_{0.1}Sb_{0.9})_{1.9}Te_3$ thin films, respectively, at the V and Cr $L_{2,3}$ edges, taken at temperatures above (hollow circles) and below (full circles) T_C. The contribution of the Te $M_{4,5}$ edges to the Cr $L_{2,3}$ spectrum is pointed out by the arrows in **b**. The XMCD spectra (black circles) were measured in the remanent state, at 5 K, demonstrating a FM state for both systems. The small dip in the pre-edge of the Cr L_3 XMCD is attributed to the induced magnetic moment in the Te atoms.

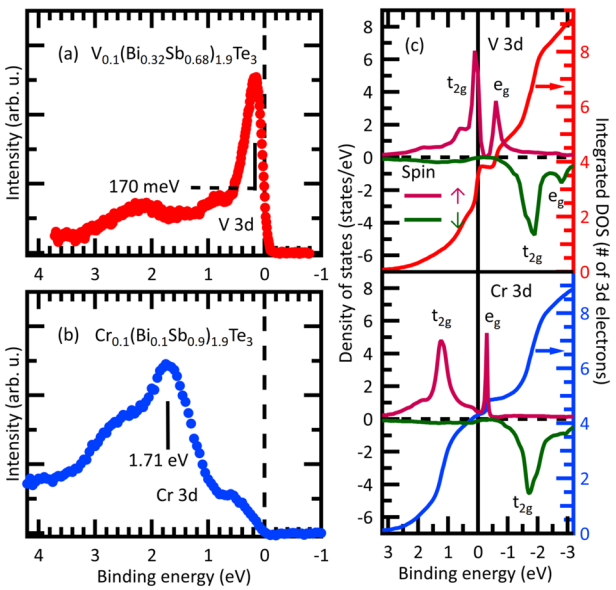

Fig. 2 Electronic structure of V and Cr impurities in (Bi,Sb)$_2$Te$_3$. resPES spectra at the L_3 edges of **a** V ($h\nu = 515$ eV) in $V_{0.1}(Bi_{0.32}Sb_{0.68})_{1.9}Te_3$ and **b** Cr ($h\nu = 575.6$ eV) in $Cr_{0.1}(Bi_{0.1}Sb_{0.9})_{1.9}Te_3$ thin films, at 30 K. **c** Calculated spin-up (magenta curves) and spin-down (green curves) 3*d* DOS and corresponding integrated DOS for substitutional V and Cr single impurities in Sb_2Te_3. The t_{2g} and e_g manifolds are identified. The integrated DOS at E_F give a total number of 3*d* electrons in the ground state of $d^{3.4}$ for V and $d^{4.4}$ for Cr.

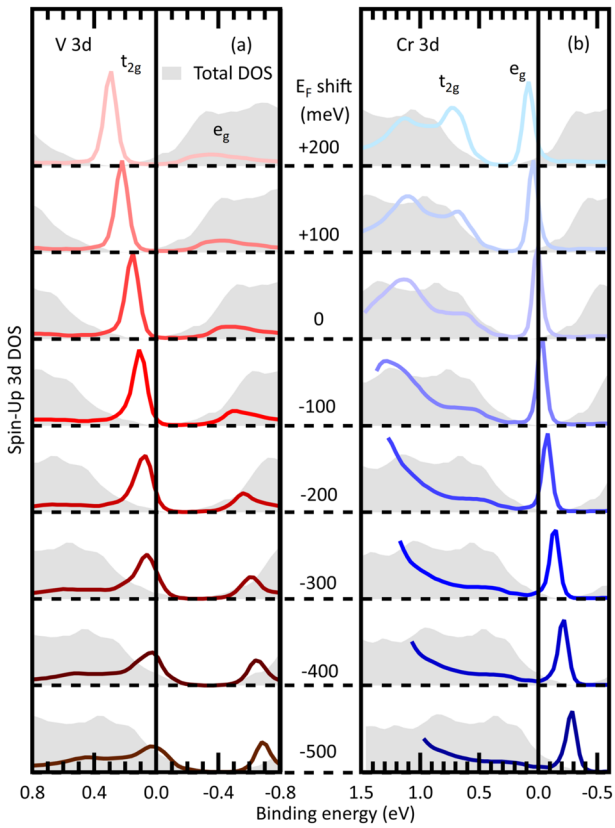

Fig. 3 Effect of charge doping on the 3*d* impurity states. Spin-up partial 3*d* DOS of **a** V and **b** Cr impurities embedded in Sb_2Te_3, calculated for different positions of E_F in respect to the bulk VB and CB. The grey shaded areas correspond to the bulk total DOS of the Sb_2Te_3 host.

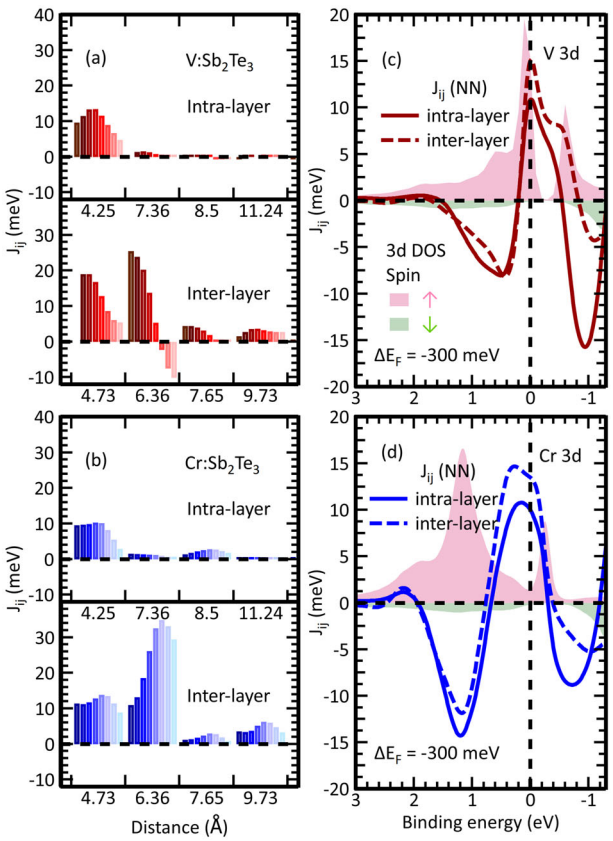

Fig. 4 Magnetic interactions in V-doped and Cr-doped Sb_2Te_3. Intra-layer (upper panels) and inter-layer (lower panels) exchange coupling constants J_{ij} as a function of distance from the **a** V and **b** Cr impurities, calculated for the same ΔE_F values as in Fig. 3 (note the corresponding colour code). Energy dependence of the NN intra-layer (solid line) and inter-layer (dashed line) $J_{ij}(E)$ in **c** V:Sb_2Te_3 and **d** Cr:Sb_2Te_3, for $\Delta E_F = -300$ meV. The corresponding spin-resolved 3*d* DOS are also plotted as shaded areas.

spin-up DOS of V and Cr impurities in Sb_2Te_3, calculated for different artificial E_F shifts (ΔE_F), i.e. different positions of E_F with respect to the bulk VB and conduction band (CB) (Supplementary Fig. 3). This approach allows us to simulate the effect of *n*-type and *p*-type charge doping on the 3*d* states, i.e. the valence of the TM impurities[37]. The results for the spin-up V and Cr 3*d* DOS are shown in Fig. 3a, b, respectively. The grey-shaded areas correspond to the Sb_2Te_3 host total DOS, emphasising the position of the impurity states with respect to the bulk band gap, where the topological surface states (TSS) typically lie. We find that the position of the impurity states depends sensitively on the charge doping, shifting towards higher binding energies when going from *p*-type (dark-coloured curves) to *n*-type (light-coloured curves) doping. In particular, the narrow V 3*d* peak gradually moves away from E_F. This trend is experimentally supported by our resPES data for $(Bi_xSb_{1-x})_2Te_3$ films with different Bi concentrations *x*, which will be discussed later. For higher *x*, and thus higher *n*-doping[3,15,16], the V 3*d* peak shifts to significantly higher binding energies.

Impurity-state-mediated magnetic exchange interactions

Based on our findings regarding the local electronic and magnetic impurity configurations, we now discuss their implications for the magnetic exchange interactions. In Fig. 4a, b we plot the calculated exchange-coupling constants J_{ij} for different separation distances between two TM ions located in one atomic plane (intra-layer coupling, upper panels) and at neighbouring atomic planes within the same quintuple layer (inter-layer coupling, lower panels), using the same ΔE_F values as in Fig. 3a, b (note the corresponding colour code). For both V and Cr, the interlayer coupling is dominant, in good agreement with ref. [17]. Overall, at nearest-neighbour (NN) distances the calculated J_{ij} contributions are larger for V, while at the second and third neighbour positions the J_{ij} values for Cr are markedly larger. This behaviour follows the spatial decay of the calculated impurity-induced features in the 3*d* DOS (Supplementary Fig. 7). Most importantly, we find that J_{ij} strongly varies with charge doping. Already small shifts of E_F give rise to considerable changes in J_{ij}, whose sign and strength are linked to characteristic features in the 3*d* DOS at E_F. For V, J_{ij} rapidly decreases in the *n*-doped regime, while for Cr the behaviour is more complex and depends more strongly on the relative impurity positions. Figure 4c, d show the energy dependence of $J_{ij}(E)$ for NN spins for $\Delta E_F = -300$ meV, which best corresponds to our experimental resPES data. The inter-layer and intra-layer components are, respectively, depicted as dashed and solid lines, and they exhibit qualitatively similar trends. In the same plots, the corresponding spin-up and spin-down 3*d* DOS are shown as shaded areas. For V, $J_{ij}(E)$ near E_F consists of a sharp peak overlapping with a broad flat ridge that spans between the onsets of the t_{2g} and e_g peaks. $J_{ij}(E)$ is maximum when E_F is positioned inside the V t_{2g} manifold, and rapidly decreases otherwise. For Cr, the sharp peak in $J_{ij}(E)$ is absent, and only the broad ridge is seen. In sharp contrast to V, we find for Cr a maximal $J_{ij}(E)$ when E_F lies in the gap between the t_{2g} and e_g peaks, where the 3*d* DOS is low. The calculated $J_{ij}(E)$ in Fig. 4d, thus, indicates a less pronounced dependence of the magnetic coupling on the E_F position for Cr. This may explain the stronger gate-voltage dependence of the

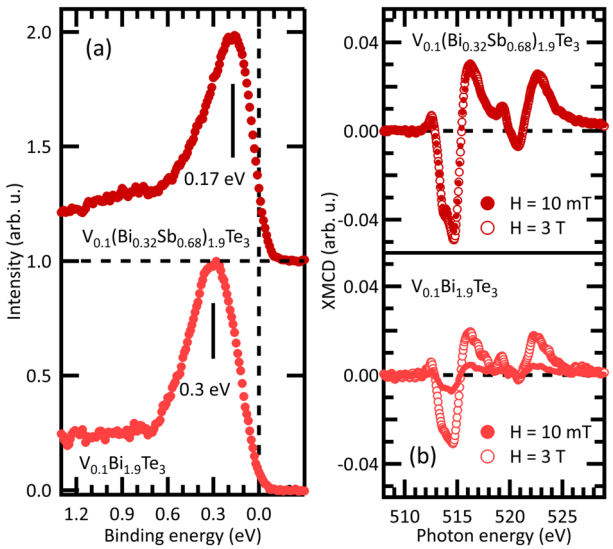

Fig. 5 Effect of the 3*d* impurity states on the magnetic properties of V:$(Bi,Sb)_2Te_3$. a resPES spectra of the V 3*d* states from $V_{0.1}(Bi_{0.32}Sb_{0.68})_{1.9}Te_3$ (dark red curve) and $V_{0.1}Bi_{1.9}Te_3$ (light red curve) thin films. The V 3*d* peak is shifted from $E_B = 170$ meV in the former to $E_B = 300$ meV in the latter. **b** V $L_{2,3}$ XMCD spectra from the same samples in **a**, taken at remanence (full circles) and saturation (hollow circles), at 5 K.

magnetic properties observed in V-doped[3] as compared to Cr-doped films[1,12,29]. These distinct features in the V and Cr 3*d* DOS are fully in line with our resPES measurements in Fig. 2. In the context of dilute magnetic semiconductors, similar characteristics in the exchange coupling constants have been extensively discussed[19,20,23,24,38–40]. By comparison, we may tentatively associate the sharp peak in $J_{ij}(E)$ for V with the double-exchange mechanism[14,17,19,20,22,24,31] and the broad ridge, found for both dopant types, with the FM superexchange mechanism[13,19,23,38].

Effect of the host charge doping on the impurity 3*d* states

In order to verify the predicted trends of the impurity-mediated magnetic exchange interactions with the charge doping of the host, we now discuss the effect of the host stoichiometry on the local electronic and magnetic properties of V-doped $(Bi_xSb_{1-x})_2Te_3$ via Bi/Sb substitution. Our resPES and XMCD data from $V_{0.1}(Bi_{0.32}Sb_{0.68})_{1.9}Te_3$ (dark red curve) and $V_{0.1}Bi_{1.9}Te_3$ (light red curve) in Fig. 5 demonstrate the strong sensitivity of the magnetic coupling on the position of the V impurity states. The V 3*d* maximum in Fig. 5a is found at $E_B = 170$ meV in the former, and at $E_B = 300$ meV in the latter ($E_B = 130$ meV for $x = 0.24$, as seen in Supplementary Fig. 2), confirming the trend predicted by our DFT calculations (Fig. 3). This may be attributed to the effect of CT from the Bi ions into the V impurities (Supplementary Fig. 4)[15,16,41]. Figure 5b shows a comparison of V $L_{2,3}$ XMCD spectra for the same samples, measured at saturation (hollow circles) and in remanence (full circles) at 5 K. While in Sb-rich V:$(Bi,Sb)_2Te_3$ the remanent and saturated spectra almost coincide, in $V_{0.1}Bi_{1.9}Te_3$ the remanent XMCD is critically lower than in saturation, demonstrating a suppression of FM interactions coinciding with the shift of the V states away from E_F, as predicted in our theoretical calculations.

DISCUSSION

The observed weakening of the ferromagnetism upon Bi doping in V:$(Bi,Sb)_2Te_3$ is in agreement with previous works[3,28,31], as well reported for single-crystalline Cr:$(Bi,Sb)_2Te_3$[26]. It is known from recent XMCD studies[18,26,29,31,32] that the Sb ions become partially polarised in the presence of substitutional V or Cr, while Bi, on the other hand, does not. Thus, our findings are consistent with a scenario where loosely localised, spin-polarised holes in Sb ions facilitate a longer ranged magnetic coupling in both systems[13,19–22]. The substitution of Sb by Bi, thus, gradually disables the network of spin-polarised *p* orbitals that contribute to stabilise a more robust FM state.

Our results yet show that the sharp V and Cr resonances are mostly localised inside the bulk band gap (see Fig. 3), indicating a considerable overlap with the TSS. While the effect of the TSS on the magnetic interactions has not been explored here, our theory suggests that the scenario pictured in the bulk may possibly be affected by the presence of the Dirac electrons at the surface, potentially leading to modified magnetic properties as compared to the bulk.

In conclusion, our systematic experimental and theoretical results highlight the central role of impurity-state-mediated exchange coupling for the magnetism in the paradigmatic QAH insulators Cr:$(Bi,Sb)_2Te_3$ and V:$(Bi,Sb)_2Te_3$. The latter cannot be explained based solely on the van Vleck mechanism, bearing its origin on the topologically non-trivial band structure[10–12]. Instead, our theoretical calculations on the basis of *pd* hybridisation and exchange coupling unambiguously elucidate the experimental observations. They show that the nature and strength of the magnetic exchange coupling vary with the position of E_F in the 3*d* DOS, i.e. with the occupation of the 3*d* states, thereby reconciling, in a unified theory, the differences observed between V and Cr doping of $(Bi_xSb_{1-x})_2Te_3$ films, as well as unveiling the role of Sb in mediating a robust ferromagnetism in QAH insulators. The presence of the Dirac states might as well have further impact on the charge and magnetic ground states of 3*d* impurities in the vicinity of the surface and, consequently, on the *pd* magnetic interactions[37]. Conversely, the 3*d* impurity states may mediate spin scattering channels for the spin-momentum-locked Dirac electrons[36]. This advance in the knowledge on the microscopic electronic and magnetic properties in V-doped and Cr-doped (Bi, $Sb)_2Te_3$ may eventually facilitate an improved understanding of the microscopic origin of the QAH effect in these systems. Finally, the developed theory can be further applied to other instances of MTI for tailoring the properties of these materials in regard to potential spintronic applications.

METHODS

Sample preparation, structural, transport and magnetic characterisation

Thin films (about 9–10 nm thick) of $Cr_z(Bi_xSb_{1-x})_{2-z}Te_3$ and $V_z(Bi_xSb_{1-x})_{2-z}Te_3$ were grown by molecular beam epitaxy (MBE) on hydrogen-passivated Si(111) substrates. The growth details and characterisation, e.g. by X-ray diffraction, atomic force microscopy and Hall magnetotransport, confirming the realisation of QAH effect in the V-doped samples (for $x = 0.76–0.79$ and $z = 0.1–0.2$), are published elsewhere[5,28,42,43]. After growth, the films were capped by a protective Te layer (~100 nm), which was mechanically removed in UHV conditions, prior to the spectroscopic measurements, revealing a chemically clean surface (Supplementary Fig. 8). Recent results have demonstrated the effectiveness of this decapping method on Bi_2Te_3 layers with high pristine quality[44]. The stoichiometries applied in this work are comparable to those that exhibited a stable and reproducible QAH effect.

XAS, XMCD and resPES

The XAS and XMCD data was acquired at the HECTOR endstation, located at BOREAS beamline of the ALBA storage ring (Barcelona, Spain)[45]. The measurements were performed in total electron yield mode, under magnetic fields of up to 6 T and temperatures down to 5 K. The resPES experiments were conducted at the ASPHERE III endstation located at beamline P04 of the PETRA III storage ring of DESY (Hamburg, Germany). The on-resonant and off-resonant VB photoemission spectra were taken at $h\nu_{on} = 514.8$ eV and $h\nu_{off} = 508$ eV for V-doped samples, and at $h\nu_{on} = 575.6$ eV and $h\nu_{off} = 560$ eV for Cr-doped ones, according to the respective XAS spectra in Fig. 1. The energy resolution of the resPES measurements

was typically better than 67 meV. All experiments were performed in ultra-high vaccuum (UHV) at pressures below 3×10^{-10} mbar.

DFT calculations

The Sb_2Te_3 and Bi_2Te_3 bulk crystals were simulated using the experimental bulk lattice structure (see ref. [46] for Sb_2Te_3 and ref. [47] for Bi_2Te_3). The electronic structure was calculated within the local density approximation (LDA)[48] to DFT by employing the full-potential relativistic Korringa–Kohn–Rostoker Green's function method (KKR)[49,50] with exact description of the atomic cells[51,52]. The truncation error arising from an $\ell_{max} = 3$ cutoff in the angular momentum expansion was corrected for using Lloyd's formula[53]. The V and Cr defects, together with a charge-screening cluster comprising the first two shells of neighbouring atoms (consisting of about 20 surrounding scattering sites), were embedded self-consistently using the Dyson equation in the KKR method[50] and have been chosen to occupy the substitutional Sb/Bi position in the quintuple layers and structural relaxations were neglected, while keeping the direction of the impurity's magnetic moment fixed along the out-of-plane direction. The shift in the Fermi level occurring in $(Bi,Sb)_2Te_3$ was accounted for by adjusting the self-consistently computed Fermi level of the host systems in the impurity embedding step. The exchange interactions among two impurities were computed using the method of infinitesimal rotations[54], which map the exchange interaction to the Heisenberg Hamiltonian $\mathcal{H} = -\frac{1}{2}\sum_{\langle ij \rangle} J_{ij} \vec{s_i} \cdot \vec{s_j}$.

MLFT calculations

Theoretical XAS and XMCD spectra for the $L_{2,3}$ ($2p \rightarrow 3d$) absorption edges of V and Cr ions were calculated by means of a configuration interaction (CI) cluster model, considering the central TM ion surrounded by six ligands (Te anions). We take into account all the $2p-3d$ and $3d-3d$ electronic Coulomb interactions, as well as the SOC on every open shell of the absorbing atom. We consider nominal $2p^6 3d^n$ ($n = 2$ for $V^{3+}$and $n = 3$ for Cr^{3+}) configurations and further include three more CT states $d^{n+1}\underline{L}^1$, $d^{n+2}\underline{L}^2$ and $d^{n+3}\underline{L}^3$ ($\underline{L}^1$ denotes a hole in the Te $5p$ orbitals) to account for hybridisation effects. To perform the CI calculation, the following fit parameters were introduced: scaling parameter β for the Hartree–Fock values of the Slater integrals, the CT energy Δ, the Coulomb interaction energy U_{dd} between the $3d$ electrons, the hybridisation energy V_{eg} and the octahedral crystal field parameter $10Dq$. The simulations were performed using the *Quanty* software for quantum many-body calculations, developed by M. W. Haverkort et al.[55]. We assume V/Cr ions embedded in the cation sites and describe the crystal field in O_h symmetry, with C_4 axes of the octahedron along the V–Te bonds. The spectral contributions from each of the split ground state terms to the absorption spectra were weighted by a Boltzmann factor. The calculated spectra were broadened by a Gaussian function to account for the instrumental broadening and by an energy-dependent Lorentzian profile for intrinsic lifetime broadening.

DATA AVAILABILITY

The data published in this work can be made available by the authors upon justified request.

CODE AVAILABILITY

The computer codes and algorithms used in this study can be provided by the authors upon justified request.

Received: 23 May 2020; Accepted: 27 October 2020;
Published online: 19 November 2020

REFERENCES

1. Chang, C.-Z., Zhang, J., Feng, X., Shen, J. & Zhang, Z. et al. Experimental observation of the quantum anomalous Hall effect in a magnetic topological insulator. *Science* **340**, 167–170 (2013).
2. Kou, X., Fan, Y., Lang, M., Upadhyaya, P. & Wang, K. L. Magnetic topological insulators and quantum anomalous Hall effect. *Solid State Commun.* **215-216**, 34–53 (2015).
3. Chang, C.-Z., Zhao, W., Kim, D. Y., Zhang, H. & Assaf, B. A. et al. High-precision realization of robust quantum anomalous Hall state in a hard ferromagnetic topological insulator. *Nat. Mater.* **14**, 473–477 (2015).
4. Bestwick, A. J., Fox, E. J., Kou, X., Pan, L. & Wang, K. L. et al. Precise quantization of the anomalous Hall effect near zero magnetic field. *Phys. Rev. Lett.* **114**, 187201 (2015).
5. Grauer, S., Schreyeck, S., Winnerlein, M., Brunner, K. & Gould, C. et al. Coincidence of superparamagnetism and perfect quantization in the quantum anomalous Hall state. *Phys. Rev. B* **92**, 201304(R) (2015).
6. Tokura, Y., Yasuda, K. & Tsukazaki, A. Magnetic topological insulators. *Nat. Rev. Phys.* **1**, 126–143 (2019).
7. Xiao, D., Jiang, J., Shin, J.-H., Wang, W. & Wang, F. et al. Realization of the axion insulator state in quantum anomalous Hall sandwich heterostructures. *Phys. Rev. Lett.* **120**, 056801 (2018).
8. Götz, M., Fijalkowski, K. M., Pesel, E., Hartl, M. & Schreyeck, S. et al. Precision measurement of the quantized anomalous Hall resistance at zero magnetic field. *Appl. Phys. Lett.* **112**, 072102 (2018).
9. Fan, Y., Upadhyaya, P., Kou, X., Lang, M. & Takei, S. et al. Magnetization switching through giant spin–orbit torque in a magnetically doped topological insulator heterostructure. *Nat. Mater.* **13**, 699–704 (2014).
10. Yu, R., Zhang, W., Zhang, H.-J., Zhang, S.-C. & Dai, X. et al. Quantized anomalous Hall effect in magnetic topological insulators. *Science* **329**, 61–64 (2010).
11. Li, M., Chang, C.-Z., Wu, L., Tao, J. & Zhao, W. et al. Experimental verification of the Van Vleck nature of long-range ferromagnetic order in the vanadium-doped three-dimensional topological insulator Sb_2Te_3. *Phys. Rev. Lett.* **114**, 146802 (2015).
12. Chang, C.-Z., Zhang, J., Liu, M., Zhang, Z. & Feng, X. et al. Thin films of magnetically doped topological insulator with carrier-independent long-range ferromagnetic order. *Adv. Mater.* **25**, 1065–1070 (2013).
13. Kim, J., Jhi, S.-H., MacDonald, A. H. & Wu, R. Ordering mechanism and quantum anomalous Hall effect of magnetically doped topological insulators. *Phys. Rev. B* **96**, 140410(R) (2017).
14. Kim, J., Wang, H. & Wu, R. Importance of coulomb correlation on the quantum anomalous Hall effect in V-doped topological insulators. *Phys. Rev. B* **97**, 125118 (2018).
15. Zhang, J.-M., Zhu, W., Zhang, Y., Xiao, D. & Yao, Y. Tailoring magnetic doping in the topological insulator Bi_2Se_3. *Phys. Rev. Lett.* **109**, 266405 (2012).
16. Zhang, J.-M., Ming, W., Huang, Z., Liu, G.-B. & Kou, X. et al. Stability, electronic, and magnetic properties of the magnetically doped topological insulators Bi_2Se_3, Bi_2Te_3, and Sb_2Te_3. *Phys. Rev. B* **88**, 235131 (2013).
17. Vergniory, M. G., Otrokov, M. M., Thonig, D., Hoffmann, M. & Maznichenko, I. V. et al. Exchange interaction and its tuning in magnetic binary chalcogenides. *Phys. Rev. B* **89**, 165202 (2014).
18. Islam, M. F., Canali, C. M., Pertsova, A., Balatsky, A. & Mahatha, S. K. et al. Systematics of electronic and magnetic properties in the transition metal doped Sb_2Te_3 quantum anomalous Hall platform. *Phys. Rev. B* **97**, 155429 (2018).
19. Kacman, P. Spin interactions in diluted magnetic semiconductors and magnetic semiconductor structures. *Semicond. Sci. Technol.* **16**, R25–R39 (2001).
20. Sato, K., Dederichs, P. H., Katayama-Yoshida, H. & Kudrnovský, J. Exchange interactions in diluted magnetic semiconductors. *J. Phys.: Cond. Matter* **16**, S5491–S5497 (2004).
21. Schulthess, T. C., Temmerman, W. M., Szotek, Z., Butler, W. H. & Malcolm Stocks, G. Electronic structure and exchange coupling of Mn impurities in III–V semiconductors. *Nat. Mater.* **4**, 838–844 (2005).
22. Jungwirth, T., Sinova, J., Mašek, J., Kučera, J. & MacDonald, A. H. Theory of ferromagnetic (III,Mn)V semiconductors. *Rev. Mod. Phys.* **78**, 809–864 (2006).
23. Sato, K., Bergqvist, L., Kudrnovský, J., Dederichs, P. H. & Eriksson, O. et al. First-principles theory of dilute magnetic semiconductors. *Rev. Mod. Phys.* **82**, 1633–1690 (2010).
24. Dietl, T. & Ohno, H. Dilute ferromagnetic semiconductors: physics and spintronic structures. *Rev. Mod. Phys.* **86**, 187–251 (2014).
25. Figueroa, A. I., van der Laan, G., Collins-McIntyre, L. J., Zhang, S.-L. & Baker, A. A. et al. Magnetic Cr doping of Bi_2Se_3: evidence for divalent Cr from x-ray spectroscopy. *Phys. Rev. B* **90**, 134402 (2014).
26. Ye, M., Li, W., Zhu, S., Takeda, Y. & Saitoh, Y. et al. Carrier-mediated ferromagnetism in the magnetic topological insulator Cr-doped $(Sb,Bi)_2Te_3$. *Nat. Comm.* **6**, 8913 (2015).
27. Gupta, S., Kanai, S., Matsukura, F. & Ohno, H. Magnetic and transport properties of Sb_2Te_3 doped with high concentration of Cr. *Appl. Phys. Express* **10**, 103001 (2017).
28. Winnerlein, M., Grauer, S., Rosenberger, S., Fijalkowski, K. M. & Gould, C. et al. Epitaxy and structural properties of $(V,Bi,Sb)_2Te_3$ layers exhibiting the quantum anomalous hall effect. *Phys. Rev. Mater.* **1**, 011201(R) (2017).
29. Duffy, L. B., Figueroa, A. I., Gładczuk, Ł., Steinke, N. J. & Kummer, K. et al. Magnetic proximity coupling to Cr-doped Sb_2Te_3 thin films. *Phys. Rev. B* **95**, 224422 (2017).
30. Duffy, L. B., Figueroa, A. I., van der Laan, G. & Hesjedal, T. Codoping of Sb_2Te_3 thin films with V and Cr. *Phys. Rev. Mater.* **1**, 064409 (2017).
31. Ye, M. et al. Negative Te spin polarization responsible for ferromagnetic order in the doped topological insulator $V_{0.04}(Sb_{1-x}Bi_x)_{1.96}Te_3$. *Phys. Rev. B* **99**, 144413 (2019).

32. Tcakaev, A., Zabolotnyy, V., Green, R. J., Peixoto, T. R. F. & Stier, F. et al. Comparing magnetic ground-state properties of the V- and Cr-doped topological insulator $(Bi,Sb)_2Te_3$. *Phys. Rev. B* **101**, 045127 (2020).
33. Peixoto, T. R. F., Bentmann, H., Schreyeck, S., Winnerlein, M. & Seibel, C. et al. Impurity states in the magnetic topological insulator $V:(Bi,Sb)_2Te_3$. *Phys. Rev. B* **94**, 195140 (2016).
34. Krieger, J. A., Chang, C. Z., Husanu, M.-A., Sostina, D. & Ernst, A. et al. Spectroscopic perspective on the interplay between electronic and magnetic properties of magnetically doped topological insulators. *Phys. Rev. B* **96**, 184402 (2017).
35. Zhang, W., West, D., Lee, S. H., Qiu, Y. & Chang, C.-Z. et al. Electronic fingerprints of Cr and V dopants in the topological insulator Sb_2Te_3. *Phys. Rev. B* **98**, 115165 (2018).
36. Sumida, K., Kakoki, M., Reinmann, J., Nurmamat, M. & Goto, S. et al. Magnetic-impurity-induced modifications to ultrafast carrier dynamics in the ferromagnetic topological insulators $Sb_{2-x}V_xTe_3$. *New J. Phys.* **21**, 093006 (2019).
37. Rüßmann, P., Mahatha, S. K., Sessi, P., Valbuena, M. A. & Bathon, T. et al. Towards microscopic control of the magnetic exchange coupling at the surface of a topological insulator. *J. Phys. Mater.* **1**, 015002 (2018).
38. Belhadji, B., Bergqvist, L., Zeller, R., Dederichs, P. H. & Sato, K. et al. Trends of exchange interactions in dilute magnetic semiconductors. *J. Phys.: Condens. Matter* **19**, 436227 (2007).
39. Larson, P. & Lambrecht, W. R. L. Electronic structure and magnetism in Bi_2Te_3, Bi_2Se_3, and Sb_2Te_3 doped with transition metals (Ti–Zn). *Phys. Rev. B* **78**, 195207 (2008).
40. Dietl, T. A ten-year perspective on dilute magnetic semiconductors and oxides. *Nat. Mater.* **9**, 965–974 (2010).
41. Zhang, J., Chang, C.-Z., Zhang, Z., Wen, J. & Feng, X. et al. Band structure engineering in $(Bi_{1-x}Sb_x)_2Te_3$ ternary topological insulators. *Nat. Commun.* **2**, 574 (2011).
42. Grauer, S., Fijalkowski, K. M., Schreyeck, S., Winnerlein, M. & Brunner, K. et al. Scaling of the quantum anomalous Hall effect as an indicator of axion electrodynamics. *Phys. Rev. Lett.* **118**, 246801 (2017).
43. Tarakina, N. V., Schreyeck, S., Duchamp, M., Karczewski, G. & Gould, C. et al. Microstructural characterization of Cr-doped $(Bi,Sb)_2Te_3$ thin films. *CrystEngComm* **19**, 3633–3639 (2017).
44. Fornari, C. I., Rappl, P. H. O., Morelhão, S. L., Peixoto, T. R. F. & Bentmann, H. et al. Preservation of pristine Bi_2Te_3 thin film topological insulator surface after *ex situ* mechanical removal of Te capping layer. *APL Mater.* **4**, 106107 (2016).
45. Barla, A., Nicolás, J., Cocco, D., Valvidares, S. M. & Herrero-Martín, J. et al. Design and performance of BOREAS, the beamline for resonant X-ray absorption and scattering experiments at the ALBA synchrotron light source. *J. Synchrotron Radiat.* **23**, 1507–1517 (2016).
46. Ullner, H.-A. Strukturuntersuchungen am System $Sb_2Te_{3-x}Se_x$ (Halbleitereigenschaften von Telluriden. VIII). *Ann. Phys.* **476**, 45–56 (1968).
47. Nakajima, S. The crystal structure of $Bi_2Te_{3-x}Se_x$. *J. Phys. Chem. Solids* **24**, 479–485 (1963).
48. Vosko, S. H., Wilk, L. & Nusair, M. Accurate spin-dependent electron liquid correlation energies for local spin density calculations: a critical analysis. *Can. J. Phys.* **58**, 1200–1211 (1980).
49. Ebert, H., Ködderitzsch, D. & Minár, J. Calculating condensed matter properties using the KKR-Green's function method—recent developments and applications. *Rep. Prog. Phys.* **74**, 096501 (2011).
50. Bauer, D. S. G. Development of a relativistic full-potential first-principles multiple scattering green function method applied to complex magnetic textures of nanostructures at surfaces. Ph.D. thesis (Forschungszentrum Jülich, RWTH Aachen University, Aachen, 2013).
51. Stefanou, N., Akai, H. & Zeller, R. An efficient numerical method to calculate shape truncation functions for Wigner–Seitz atomic polyhedra. *Comput. Phys. Commun.* **60**, 231–238 (1990).
52. Stefanou, N. & Zeller, R. Calculation of shape-truncation functions for Voronoi polyhedra. *J. Phys. Condens. Matter* **3**, 7599–7606 (1991).
53. Zeller, R. An elementary derivation of Lloyd's formula valid for full-potential multiple-scattering theory. *J. Phys. Condens. Matter* **16**, 6453–6468 (2004).
54. Liechtenstein, A., Katsnelson, M., Antropov, V. & Gubanov, V. Local spin density functional approach to the theory of exchange interactions in ferromagnetic metals and alloys. *J. Magn. Magn. Mater.* **67**, 65–74 (1987).
55. Haverkort, M. W., Zwierzycki, M. & Andersen, O. K. Multiplet ligand-field theory using Wannier orbitals. *Phys. Rev. B* **85**, 165113 (2012).

ACKNOWLEDGEMENTS

T.R.F.P. would like to thank Kai Fauth and Arthur Ernst for their collaboration at early phases of this study. H.B. would like to thank Ján Minár, and P.R. would like to thank Peter Dederichs for helpful discussions. P.R. and S.B. acknowledge funding from the Priority Programme SPP-1666 Topological Insulators of the Deutsche Forschungsgemeinschaft (DFG) (projects MA4637/3-1) and from the VITI Programme of the Helmholtz Association, as well as computing time granted by the JARA Vergabegremium and provided on the JARA Partition part of the supercomputer CLAIX at RWTH Aachen University. R.J.G. was supported by the Natural Sciences and Engineering Research Council of Canada. The experiments at the BOREAS beamline of ALBA Synchrotron were performed under the proposal-ID 2017082310, with the collaboration of ALBA staff. We acknowledge the financial support from the Deutsche Forschungsgemeinschaft (DFG) through the SFB1170 'ToCoTronics' (project No. 258499086, projects A01, B01 and C06), and the Würzburg-Dresden Cluster of Excellence on Complexity and Topology in Quantum Matter - *ct.qmat* (EXC 2147, project-id 39085490). Funding for the photoemission spectroscopy instrument at beamline P04 (Contracts 05KS7FK2, 05K10FK1, 05K12FK1, and 05K13FK1 with Kiel University; 05KS7WW1 and 05K10WW2 with Würzburg University) by the Federal Ministry of Education and Research (BMBF) is gratefully acknowledged.

AUTHOR CONTRIBUTIONS

T.R.F.P. wrote the paper, with support of H.B., P.R. and A.-V.T. M.W. and S. Schreyeck synthesised and characterised the samples under the supervision of C.G. and K.B. T.R. F.P., A.-V.T., R.C.V., S. Schatz, F.S., H.M. and A.B. performed the XAS and XMCD measurements. T.R.F.P., A.-V.T., V.Z. and A.B. analysed the XAS and XMCD data. A.-V.T., V.Z., R.J.G. and F.S. performed the MLFT calculations under the supervision of V.H. P.R. performed the DFT calculations under the supervision of S.B. T.R.F.P., H.B., S. Schatz, R.C.V., C.I.F. and C.H.M. performed the resPES experiments. T.R.F.P., R.C.V. and S. Schatz performed the resPES data analysis. A.B., H.B.V., P.G. and M.V. gave scientific and technical support during the XAS/XCMD experimental sessions at the BOREAS endstation, at ALBA. J.B., M.H., F.D., S.R. and M.K. gave scientific and technical support during the resPES experiments at the P04 beamline, at PETRA-III, DESY. K.R., S.B., V.H, L.W.M. and F.R. jointly supervised the work. All authors contributed in the discussions and interpretation of the results.

FUNDING

Open Access funding enabled and organized by Projekt DEAL.

COMPETING INTERESTS

The authors declare no competing interests.

ADDITIONAL INFORMATION

Supplementary information is available for this paper at https://doi.org/10.1038/s41535-020-00288-0.

Correspondence and requests for materials should be addressed to T.R.F.P.

Reprints and permission information is available at http://www.nature.com/reprints

Publisher's note Springer Nature remains neutral with regard to jurisdictional claims in published maps and institutional affiliations.